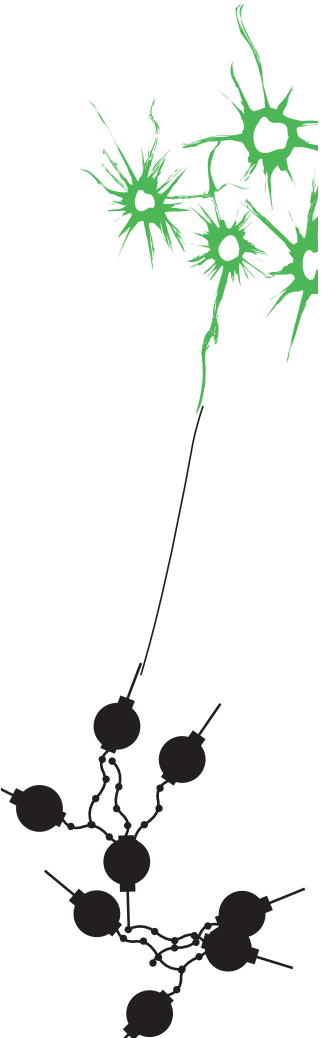

RAM ROBOTICS AND MECHATRONICS

THE SELF-SENSING PROPERTIES OF CONTINUOUS CARBON FIBER REINFORCED, 3D-PRINTED BEAMS AS FUNCTION OF THE NUMBER OF REINFORCED PERIMETERS

J.C. (Jonathan) Schaaij

BSC ASSIGNMENT

Committee:
prof. dr. ir. G.J.M. Krijnen
ir. A.P. Dijkshoorn
dr. ir. W.J.B. Grouve

July, 2022

021RaM2022
Robotics and Mechatronics
EEMCS
University of Twente
P.O. Box 217
7500 AE Enschede
The Netherlands

UNIVERSITY OF TWENTE. | TECHMED CENTRE UNIVERSITY OF TWENTE. | DIGITAL SOCIETY INSTITUTE

Contents

Self-sensing properties of continuous carbon fiber reinforced, 3D-printed beams

Jonathan Schaaij, Alexander Dijkshoorn, Stefano Stramigioli, Gijs Krijnen
Robotics and Mechatronics Group, University of Twente, Enschede, the Netherlands
a.p.dijkshoorn@utwente.nl

***Abstract*—This paper investigates self-sensing properties of continuous carbon fiber reinforced, 3D-printed beams as function of the number of reinforced perimeters. Samples containing various numbers of fiber reinforced perimeters have been tested for their stiffness and strain-dependent resistance using three-point-bending tests. The mechanical properties are modelled successfully using classical beam theory and the resistance of the printed part can be estimated using the resistance of the fiber additive. Large resistance changes are measured during bending tests, which results in an overall high sensitivity. More research is required to determine a conclusive relation between the number of reinforcement fibers and piezoresistive sensitivity for bending.**

***Index Terms*—3D-Printing, continuous carbon fiber, composite fiber co-extrusion, self-sensing structures, strain gauge**

I. Introduction

A novel method in fused filament fabrication (FFF) called composite fiber co-extrusion (CFC) makes it possible to 3D-print continuous carbon fiber (CCF). Using this method a thermoplastic polymer is extruded around the fiber, embedding it inside the printed part [1]. The embedded fiber provides excellent mechanical properties crucial to make light, stiff and strong components [2]. Additionally, CCF is electrically conductive and has piezoresistive properties, which can be used for sensing [3], [4]. Previous research has shown that, combined with the geometric degrees of freedom provided by FFF 3D-printing, CCF can be used to print electrical circuits [5]. The piezoresistive properties make it possible to use CCF for self-sensing structures, in which the fibers provide mechanical strength as well as measuring possibilities [6], [7]. These offer numerous advantages over traditional separate sensors, such as a simplified manufacturing process and distributed sensing of large-scale structures. Luan et al. [8], [9] showed that such self-sensing structures can function as a strain gauge measuring a linear reversible resistance increase for elastic deformation. Beyond the elastic regime larger irreversible resistance changes can be used as an indication for structural damage. To the authors knowledge, there have been no papers investigating the influence of the fiber-volume fraction on the performance of 3D-printed CCF strain gauges. Therefore, this paper presents the electrical and mechanical characterization of 3D-printed self-sensing CCF reinforced structure with various numbers of reinforced perimeters. Models are presented followed by an explanation of the experimental methods. Finally the results are shown and discussed.

This work was partially developed within the PortWings project, funded by the European Research Council under Grant Agreement No. 787675.

II. Theory

A. Mechanical Model

The tested samples are beams containing CCF perimeters in the top and bottom layers, where they provide the maximum stiffness, as seen in Figure 1. A mechanical model is required to determine the strain of the fibers during the three-point-bending test. Since the beam contains different materials at different locations, the beam model is split into five layers with varying material volume fractions.

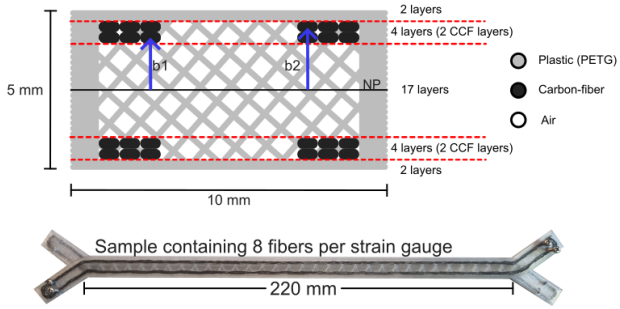

Fig. 1. Cross-section of the 3D-printed beams containing two strain gauges, made up of two fiber layers at distance b_1 and b_2 from the neutral plane (NP) and three reinforced perimeters, as well as the sections for the mechanical model indicated by the red lines (top). Picture of a printed beam containing two CCF strain gauges (bottom)

Using the rule of mixtures [10] the effective Young's moduli for each section can be determined, where the volume fraction of air is assumed to have no contribution to the overall strength. Furthermore, the transformed section method [11] determines the area moment of inertia.

The center deflection $y_{\max}$ during a three-point-bending test [12] and the stiffness k of the samples can be calculated using the following equations:

$$y_{\max} = \frac{FL^3}{48EI} \qquad k = \frac{F}{y_{\max}} = \frac{48EI}{L^3} \tag{1}$$

Where F is the applied force, L is the distance between the supports in the bending test and E and I are the effective Young's modulus and the area moment of inertia of the beam respectively.

The average strain $\bar{\epsilon}$ along the fibers located a distance b away from the neutral plane can be calculated by integrating the local strain over the length of the beam determined by the bending radius $\rho(x)$:

$$\bar{\epsilon} = \frac{2}{L}\int_0^{\frac{L}{2}} \frac{b}{\rho(x)}dx = \frac{bFL}{8EI} = \frac{6by_{\max}}{L^2} \tag{2}$$

B. Electrical Model

A common problem with CCF strain gauges are the electrodes, which often have a significant contact resistance [13]. To overcome this problem 4-point resistance measurements are used. Since the CCF are placed as reinforced perimeters, they form a loop as seen in Figure 1 and 2. This means that the electrodes can not be placed inline, like a conventional 4-point resistance measurement. Instead the electrodes are placed on the fiber loop resulting in two possible methods to measure the resistance with four electrodes, shown in Figure 2.

A parallel 4-point measurement (center) measures $R_{\text{parallel}} := \frac{V}{I}\big|_{\text{parallel}} = R_{\text{f}}/(1 + \frac{R_x}{2R_{\text{f}}})$ [14], whereas a diagonal 4-point measurement (right) measures $R_{\text{diagonal}} := \frac{V}{I}\big|_{\text{diagonal}} = R_{\text{f}} - \frac{R_x}{2}$, where R_{f} is the combined resistance of the two sections of fiber which make up the strain gauge and R_x is the orthogonal resistance between the current and voltage electrode on a side. For the model it is assumed that R_x is equal on both sides and not influenced by the strain acting on R_{f}, because it lies outside the bending supports. This assumption makes it possible to conclude that $\Delta R_{\text{diagonal}} = \Delta R_{\text{f}}$. Where R_{f} can be calculated as follows:

$$R_{\text{f, measured}} = R_{\text{parallel}} + \sqrt{R_{\text{parallel}}^2 - R_{\text{parallel}}R_{\text{diagonal}}} \tag{3}$$

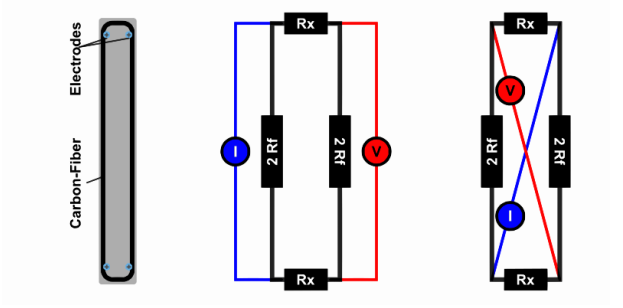

Fig. 2. Representation of fabricated sample with fiber and contact screws (left); Resistance model with parallel 4-point measurement (center); Resistance model with diagonal 4-point measurement (right)

To model the piezoresistive response the linear model made by C. Luan et. al. [9] is used as a starting point, where the change in resistance is a result of the average strain ($\bar{\epsilon}$) and the gauge factor (k): $R = R_0(1 + k\bar{\epsilon})$

This model needs to be extended for the samples containing two layers of fibers, where the ith fiber layer is located a distance b_i away from the neutral plane, as seen in Figure 1. For this model the two layers containing fibers are considered as separate resistors. First a new factor is chosen as $K = k\bar{\epsilon}/b_i$, which allows the resistances of each layer to be described as $R_i = 2R_{\text{f},0}(1 + b_iK)$, where R_i is the resistance of the ith layer and $2R_{\text{f},0}$ is the resistance of an unstrained single fiber layer. Using the equation of parallel resistances the expected strained fiber resistance can be modelled as:

$$R_{\text{f}} = \frac{R_1R_2}{R_1 + R_2} = \frac{4R_{\text{f},0}^2(1 + b_1K)\cdot(1 + b_2K)}{2R_{\text{f},0}(1 + b_1K) + 2R_{\text{f},0}(1 + b_2K))} \tag{4}$$

Finally the change in resistance can by calculated as follows:

$$\frac{\Delta R}{R_{f,0}} = \frac{R_{\text{f}} - R_{\text{f},0}}{R_{\text{f},0}} = \frac{2b_1b_2K^2 + b_1K + b_2K}{2 + b_1K + b_2K} \tag{5}$$

III. Methodology

A. Fabrication

The samples used for the experiment are beams with a rectangular cross section of $5\,\text{mm}$ by $10\,\text{mm}$ presented in Figure 1. CCF composite filament made by Anisoprint is placed symmetrically at the top and bottom of these samples, such that each sample contains two strain gauges. The symmetrical placement ensures that the neutral plane is in the center and prevents warping caused by the different coefficients of thermal expansion of PETG and CCF composite filament [15], [16].

The test samples have been printed on the Anisoprint Composer A4 [1], [2], which is an FFF 3D-Printer with a secondary extruder for composite fiber co-extrusion (CFC), extruding CCF and plastic simultaneously to embed the CCF inside the plastic. The default profiles for PETG and CCF in the slicer (Aura 1.24.2 [17]) are used to generate the G-Code for the printer, where the layer height of the is $0.17\,\text{mm}$ for the PETG, and $0.34\,\text{mm}$ for the CCF. The fibers are placed as outer reinforced perimeter, where the perimeter count determines the amount of fibers. Height range modifiers in the slicer are used to place the fibers only in the top and bottom layers, while the first two and last two layers are printed with 100% PETG. Samples with one fiber layer on each side ($N_{\text{fiber layers}} = 1$) are printed with 1 to 3 reinforced perimeters, samples with two fiber layers ($N_{\text{fiber layers}} = 2$) are printed with 1 to 4 reinforced perimeters. The number of fibers refers to the amount of fibers which make up a strain gauge and can be calculate using the following equation:

$$N_{\text{fibers}} = 2 \cdot N_{\text{fiber layers}} \cdot N_{\text{reinforced perimeters}} \tag{6}$$

Additionally samples have been printed without any fibers and with as many fibers as possible which contain a total of 120 fibers. Each sample has two outer perimeters of PETG with $20\,\%$ triangular infill.

For the electrodes a small hole ($d = 1.5\text{mm}$) is drilled right next to the fibers, such that the fibers are exposed without being damaged. Stainless steel M2 bolts are then screwed into the holes to make the electrical connection to the carbon fiber.

B. Characterization

A Keithley 2000 multi-meter and an HP34401A are used to measure the sample resistance. Parallel and diagonal 4-point measurements determine $R_{\text{f},0}$ using Equation 3.

The samples are tested on a three-point-bending setup with rounded supports ($r = 5\,\mathrm{mm}$, [18]) placed $200\,\mathrm{mm}$ apart. A load is applied at the center using a linear actuator (SMAC LCA25-050-15F) in force control mode, while also measuring the displacement of the sample. The applied load is a triangular signal from $0\,\mathrm{N}$ to $12\,\mathrm{N}$ with a period of $20\,\mathrm{s}$. A measurement lasts a total of ten periods to compensate for noise in the signal and to measure non-linear effects such as hysteresis, drift and creep. The resistance of the bottom strain gauge is measured using the diagonal 4-point resistance method under tension once normally and once upside down to measure the resistance change during compression.

A PC running Matlab is used to drive the linear actuator and save the data from the multi-meter.

By fitting the measured displacement and change in resistance to the resistance model in Equation 5 combined with the strain model in Equation 2 the gauge factor is determined.

IV. Results

The stiffness of the sample containing 120 fibers has been used to determine the Young's modulus of the printed CCF: $E_{\mathrm{CCF}} = 57.45\ \mathrm{GPa}$. The result is $43\,\%$ of the value found in the data-sheet of the CCF composite filament [1], [19]. However, this result is confirmed by the mechanical model which matches the measured sample stiffness as seen in the top plot of Figure 3. The slope of the stiffness plot being lower for the samples containing a two CCF layers matches the expectation, since the average distance from the neutral plane to the fibers is lower.

Extrapolating the resistance of the unstrained, CCF composite filament before being printed, gives the expected unstrained resistance seen in the center plot of Figure 3. While most measured unstrained resistances are slightly higher than the expectation there is a clear correlated trend. Due to unstable electrode connections under strain for the samples containing one fiber layer, the sensitivity is only determined for the two layered samples, seen in the bottom plot of Figure 3. It shows that the sensitivity of the CCF is higher in tension compared to compression. There seems to be a negative correlation between the sensitivity and the fiber count, however, this observation is not consistent as the strain gauge containing 16 fibers shows the second largest sensitivity in tension and the largest in compression.

The resistance change for the sample with two fiber layers and 4 reinforced perimeters during compression and tension can be seen in Figure 4. Large changes in resistance of over $10\,\%$ are measured, which far exceeds previous research, which only measure a resistance change of $\approx 1\,\%$ [8], [9], [20]. Similar to previous research, the piezoresistive response is not linear, showing a decreasing sensitivity for larger deflections. The resistance measurement shows significant noise levels and the right plot of Figure 4 shows a linear correlation between deflection and force, but with some hysteresis.

V. Discussion and Conclusions

This work proves experimentally that the resistance of 3D printed continuous carbon fiber beams can be controlled by varying the perimeter count. Using classical beam theory the stiffness of the beam can be predicted. Combining parallel and diagonal 4-point resistance measurements makes it possible to determine the resistance of sections along a conductive loop. Even if the orthogonal resistance R_x would be large, it would not affect the absolute change in resistance during a diagonal 4-point measurement. The sensitivity of the CCF is lower during compression compared to tensile strain. A high sensitivity of the strain gauges shows potential for highly sensitive CCF self-sensing structures. More research is required to determine a correlation between the reinforced perimeter count and the sensitivity of the self sensing structures.

In future research the influence of other slicing settings, such as the fiber extrusion multipliers or plastic infill density, will be explored. Finally practical applications will be researched, such as self-sensing robotic structures.

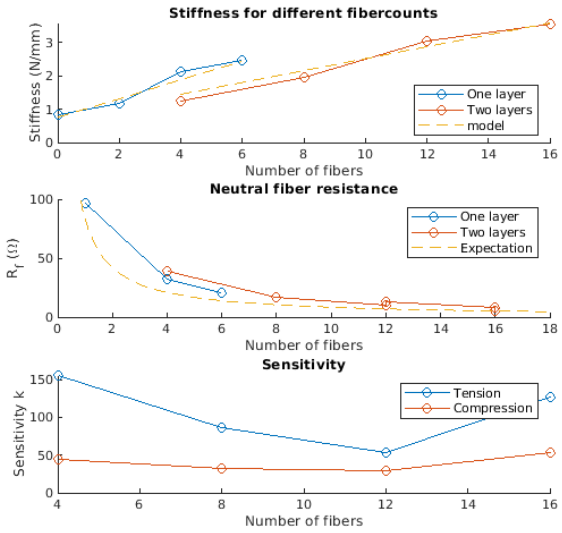

Fig. 3. Measured stiffness compared to the model (top); Fiber resistance calculated using Equation 3 compared to the expected resistance (middle); Sensitivity k of the two layered samples during compression and tension (bottom)

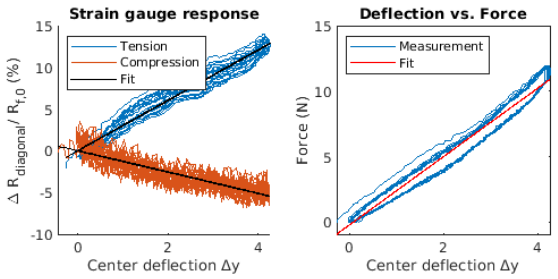

Fig. 4. Resistance response to tensile and compressive strain along with fitted result (Left). Force deflection curve showing hysteresis (Right)

REFERENCES

[1] Anisoprint, "Anisoprint Composer," https://anisoprint.com/solutions/desktop/, (accessed: 16.03.2022).

[2] A. V. Azarov, F. K. Antonov, M. V. Golubev, A. R. Khaziev, and S. A. Ushanov, "Composite 3d printing for the small size unmanned aerial vehicle structure," *Composites Part B: Engineering*, vol. 169, pp. 157–163, 2019. [Online]. Available: https://www.sciencedirect.com/science/article/pii/S1359836818320031

[3] P. Scholle and M. Sinapius, "A review on the usage of continuous carbon fibers for piezoresistive self strain sensing fiber reinforced plastics," *Journal of Composites Science*, vol. 5, no. 4, 2021. [Online]. Available: https://www.mdpi.com/2504-477X/5/4/96

[4] S. Wang and D. Chung, "Self-sensing of flexural strain and damage in carbon fiber polymer-matrix composite by electrical resistance measurement," *Carbon*, vol. 44, no. 13, pp. 2739–2751, 2006. [Online]. Available: https://www.sciencedirect.com/science/article/pii/S0008622306001928

[5] S. Swaminathan, K. B. Ozutemiz, C. Majidi, and S. E. Hudson, "Fiberwire: Embedding electronic function into 3d printed mechanically strong, lightweight carbon fiber composite objects," in *Proceedings of the 2019 CHI Conference on Human Factors in Computing Systems*, ser. CHI '19. New York, NY, USA: Association for Computing Machinery, 2019, p. 1–11. [Online]. Available: https://doi-org.ezproxy2.utwente.nl/10.1145/3290605.3300797

[6] F. Mashayekhi, J. Bardon, V. Berthé, H. Perrin, S. Westermann, and F. Addiego, "Fused filament fabrication of polymers and continuous fiber-reinforced polymer composites: Advances in structure optimization and health monitoring," *Polymers*, vol. 13, no. 5, 2021. [Online]. Available: https://www.mdpi.com/2073-4360/13/5/789

[7] M. Schouten, G. Wolterink, A. Dijkshoorn, D. Kosmas, S. Stramigioli, and G. Krijnen, "A review of extrusion-based 3d printing for the fabrication of electro-and biomechanical sensors," *IEEE Sensors Journal*, pp. 1–1, 2020.

[8] C. Luan, X. Yao, C. Liu, L. Lan, and J. Fu, "Self-monitoring continuous carbon fiber reinforced thermoplastic based on dual-material three-dimensional printing integration process," *Carbon*, vol. 140, pp. 100–111, 2018. [Online]. Available: https://www.sciencedirect.com/science/article/pii/S0008622318307498

[9] C. Luan, X. Yao, H. Shen, and J. Fu, "Self-sensing of position-related loads in continuous carbon fibers-embedded 3d-printed polymer structures using electrical resistance measurement," *Sensors*, vol. 18, no. 4, 2018. [Online]. Available: https://www.mdpi.com/1424-8220/18/4/994

[10] F. C. Campbell, *Structural composite materials*. Materials Park, Ohio: ASM International, 2010.

[11] S. K. F. Ansel C. Ugural, *Advanced Mechanics of Materials and Applied Elasticity*, 6th ed. Peasron, 8 2019.

[12] J. Hodgkinson, "7 - flexure," in *Mechanical Testing of Advanced Fibre Composites*, ser. Woodhead Publishing Series in Composites Science and Engineering, J. Hodgkinson, Ed. Woodhead Publishing, 2000, pp. 124–142. [Online]. Available: https://www.sciencedirect.com/science/article/pii/B9781855733121500111

[13] P. Scholle, S. Rüther, and M. Sinapius, "Comparison of electrical contacting techniques to carbon fiber reinforced plastics for self-strain-sensing applications," *C*, vol. 7, no. 4, 2021. [Online]. Available: https://www.mdpi.com/2311-5629/7/4/81

[14] A. Dijkshoorn, V. Ravi, P. Neuvel, S. Stramigioli, and G. Krijnen, "Mechanical interlocking for connecting electrical wires to flexible, fdm, 3d-printed conductors."

[15] SD3D, *PETG (Polyethylene terephthalate copolyester) Technical Data Sheet*, 2022.

[16] C. Dong, K. Li, Y. Jiang, D. Arola, and D. Zhang, "Evaluation of thermal expansion coefficient of carbon fiber reinforced composites using electronic speckle interferometry," *Opt. Express*, vol. 26, no. 1, pp. 531–543, Jan 2018. [Online]. Available: http://opg.optica.org/oe/abstract.cfm?URI=oe-26-1-531

[17] Anisoprint, "Aura," 7 Jun 2022. [Online]. Available: https://anisoprint.com/aura/

[18] "Iso-178 ;plastics — determination of flexural properties," 2019.

[19] Anisoprint, "Anisoprint composer - manual," 1 Jul 2022. [Online]. Available: https://support.anisoprint.com/composer/manual/

[20] X. Yao, C. Luan, D. Zhang, L. Lan, and J. Fu, "Evaluation of carbon fiber-embedded 3d printed structures for strengthening and structural-health monitoring," *Materials & Design*, vol. 114, pp. 424–432, 2017. [Online]. Available: https://www.sciencedirect.com/science/article/pii/S0264127516313879

A Theory

A.1 Introduction

This chapter elaborates on the theoretical models used in the paper.

A.2 Mechanical Model

As mentioned in the paper the mechanical model is used to determine the fiber strain, however, additional sample are tested, which only contain fiber on one side. Because those beam are not symmetrical the neutral plane shifts. This model determines the height of the neutral plane for the single side samples.

A.2.1 Area Moment of inertia

The first step to calculate bending of the beam is to calculate the area moment of inertia (I_{beam}) for the beam, which can be done using the following equation [1]:

$$I_{\text{beam}} = \int (y - y_{\text{neutral}})^2 dA \tag{A.1}$$

Where y is the height from the bottom of the part and A is the cross sectional area. However, this equation only holds for homogeneous beams. Since the sample used for the strain-gauge consists of different materials and is not homogeneous due to the 3D-printing process, the area moment of inertia needs to be calculated using a different approach. By modelling it as a multi-layer beam I_{beam} can be calculated using the transformed section method as seen in Figure A.1 [2,3]

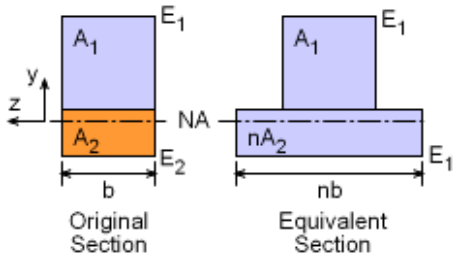

Figure A.1: Transformed section method [4]

To determine the equivalent widths of each section, the moduli of elasticity need to calculated. Each section consists of a certain volume fraction PTEG, carbon-fiber and air as seen in Figure 1.

The volume fraction of CCF v_{f} is calculated as follows:

$$v_{\text{f}} = \frac{n_{\text{f}} \cdot A_{\text{CCF filament}}}{A_{\text{section}}} \tag{A.2}$$

The volume fraction of PETG is calculated using the infill percentage and the width of the outer plastic perimeter.

For these volume fractions the PETG, which is extruded around the CCF composite filament is not included. Additionally, it assumes the infill is still printed where the carbon-fiber is. These simplifications result in opposing errors, which reduces the final error and both errors are insignificant compared the strength of the fibers.

The air is a result of the infill which leaves empty space inside the 3D-printed part. For this project it is assumed that the air inside the part does not contribute anything to the strength of the part, since the strength is insignificant.

The equivalent modulus of elasticity E_{eq} can be calculated using the following equation:

$$E_{eq} = E_p \cdot v_p + E_f \cdot v_f \tag{A.3}$$

Where v_p , v_f, E_p and E_f the the volume fractions and Young's moduli of PETG and the CCF respectively.

The equivalent width is a product of the original width with the ratio of the moduli of elasticity [3]:

$$w_{eq} = w \cdot \frac{E_{eq}}{E_p} \tag{A.4}$$

In this case E_p is chosen as the effective homogeneous Young's modulus of the equivalent beam.

The height of the neutral plane can be determined by finding the average height of all sections i of the equivalent beam:

$$y_{neutral} = \frac{\sum_{i=1}^{n} A_i \cdot y_{center_i}}{\sum_{i=1}^{n} A_i} \tag{A.5}$$

Now I_{beam} can finally be calculated by combining the area moment of inertia for each section with the parallel axis theorem [1]:

$$\begin{aligned} I_i &= \frac{w_{eq,i} \cdot h_i^3}{12} \\ I_{beam} &= \sum_{i=1}^{n} \left(I_i + A_i \cdot (y_{neutral} - y_{center,i})^2 \right) \end{aligned} \tag{A.6}$$

A.2.2 Bending Deformation

To determine the displacement of the beam, Euler-Bernouilli beam theory is used, which is valid since the cross section and the displacements are small compared to the length of the beam. The deflection of a beam can be calculated using the radius of curvature (ρ), which correlated to the beam properties and bending moment as follows [2]:

$$\frac{d^2y}{dx^2} = \frac{1}{\rho} = \frac{M}{E_p I_{beam}} \tag{A.7}$$

Ep is used in this equation as it was chosen to be the homogeneous Young's modulus to calculate I_{beam} in Equation A.4.

For a three point bending test as described in Section C.3, there are three forces acting on the beam. The actuator force F at the center and two restoring forces $F/2$ at the supports, as seen in Figure A.2.

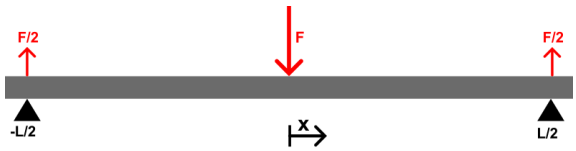

Figure A.2: Forces acting on the beam

By integrating over the force the bending moment in between the supports can be determined to be [2]:

$$M(x) = \frac{1}{2} F \left(\frac{L}{2} - x \right) \tag{A.8}$$

In this equation L corresponds to the distance between the supports and x corresponds to the absolute distance from the center of the beam.

Using double integration the actual deflection can be determined. For this two boundary conditions are required. The first boundary condition is that the maximum deflection is in the center where the force is applied:

$$\frac{dy}{dx}(0) = 0 \tag{A.9}$$

The second boundary condition is that there is no deflection at the supports:

$$y\left(\frac{L}{2}\right) = 0 \tag{A.10}$$

These boundary conditions result in the following equation for the deflection of the beam:

$$y = \frac{F}{4E_{\mathrm{p}}I_{\mathrm{beam}}}\left(\frac{L}{2}x^2 - \frac{1}{3}x^3 - \frac{L^3}{12}\right) \tag{A.11}$$

At the center of the sample, where the actual position will be measured, this equation simplifies to:

$$y(0) = y_{\max} = -\frac{FL^3}{48E_{\mathrm{p}}I_{\mathrm{beam}}} \tag{A.12}$$

A.2.3 Strain

While bending a beam the material on one side of the neutral plane will be in compression, while the other side of the neutral plane will be in tension. This means that the strain on the beam depends not only on the position x along the axis, but also on the distance from the neutral plane b [2]:

$$\epsilon(x) = \frac{b}{R(x)} = \frac{bM(x)}{E_{\mathrm{p}}I_{\mathrm{beam}}} = \frac{bF(L/2-x)}{2\cdot E_{\mathrm{p}}I_{\mathrm{beam}}} \tag{A.13}$$

The average strain at an offset b can be calculated by integrating over the local strain.

$$\bar{\epsilon} = \frac{2}{L}\int_0^{L/2}\epsilon(x)dx \quad \Longrightarrow \quad \bar{\epsilon} = -\frac{bFL}{8E_{\mathrm{p}}I_{\mathrm{beam}}} \tag{A.14}$$

Using Equation A.12 the average strain can be expressed as a function of $y_{\max}$:

$$\bar{\epsilon} = \frac{6by_{\max}}{L^2} \tag{A.15}$$

A.3 Resistance Model

The expected resistance of the beams are calculated using the resistance of the CCF filament using the equation for N_{fibers} parallel resistors:

$$R_n = \frac{1}{\frac{1}{R_{\mathrm{filament}}} + \frac{1}{R_{\mathrm{filament}}} + \ldots} = \frac{1}{\frac{1}{R_{\mathrm{filament}}}\cdot N_{\mathrm{fibers}}} = \frac{R_{\mathrm{filament}}}{N_{\mathrm{fibers}}} \tag{A.16}$$

Where N_{fibers} is determined using Equation B.1.

The equations to determine R_{f} and R_{x} are determined by first calculating the resistance between the current sources using the parallel resistor equation. This calculated resistance is then used to determine the voltage at each voltage electrode using Ohms law. Subtracting the

voltages at the electrodes and dividing by the current results in the measured resistance on a multi-meter:

$$\begin{aligned} R_{\text{diagonal}} &= R_{\text{f}} - R_{\text{x}}/2 \\ R_{\text{parallel}} &= R_{\text{f}} \frac{1}{1+\frac{R_{\text{x}}}{2R_{\text{f}}}} \end{aligned} \tag{A.17}$$

Rearranging R_{parallel} and inserting R_{x} determined by R_{diagonal} makes it possible to determine R_{f}:

$$\begin{aligned} R_{\text{parallel}} &= R_{\text{f}} \frac{1}{1+\frac{R_{\text{x}}}{2R_{\text{f}}}} \\ R_{\text{parallel}} + \frac{R_{\text{x}} R_{\text{parallel}}}{2R_{\text{f}}} &= R_{\text{f}} \\ 0 &= R_{\text{f}}^2 - R_{\text{f}} R_{\text{parallel}} - \frac{R_{\text{x}} R_{\text{parallel}}}{2} \\ R_{\text{x}} &= 2(R_{\text{f}} - R_{\text{diagonal}}) \\ 0 &= R_{\text{f}}^2 - 2R_{\text{f}} R_{\text{parallel}} - R_{\text{diagonal}} R_{\text{parallel}} \\ R_{\text{f}} &= R_{\text{parallel}} \pm \sqrt{R_{\text{parallel}}^2 - R_{\text{parallel}} R_{\text{diagonal}}} \end{aligned} \tag{A.18}$$

Due to the square root in the final equation two solutions are possible, but only the positive solution results in a physical value.

The resistance model to determine R_{f} and R_{x} relies on two assumptions. The first assumption is that the orthogonal resistance R_{x} is not influenced by the strain. This assumption is logical, since strain should only occur within the supports of the three-point-bending setup.
The second assumption is that R_{x} is the same on both sides. This assumption is not entirely correct, since the fiber forming a loop has a beginning and an end, which are not always connected as seen in Figure E.1, resulting in a higher resistance. However, this assumption is required to be able to calculate R_f. Without the equality assumption there would be three unknown variables, $R_{\text{x},1}$, $R_{\text{x},2}$, and R_f, with only two equations, one for R_{diagonal} and one for R_{parallel}. Therefore, it would not be possible to calculate any resistance.

A.4 Piezoresistive model

To model the piezoresistive response the linear model made by C. Luan et. al. [5] is used as a starting point, where the change in resistance is a result of the average strain $\bar{\epsilon}$ and the gauge factor k:

$$R = R_0(1 + k\bar{\epsilon}) \tag{A.19}$$

This model needs to be extended for the samples containing two layers of fibers, where the ith fiber layer is located a distance b_i away from the neutral plane, as seen in Figure **??**. For this model the two layers containing fibers are considered as separate resistors. First a new factor is chosen as:

$$K = k\bar{\epsilon}/b_i = \frac{6ky_{\text{max}}}{L^2} \tag{A.20}$$

The neutral fiber resistance is $R_{\text{f},0}$. For a sample containing two layers of fibers, the neutral resistance of a single layer is expressed by $2R_{\text{f},0}$, which allows the resistances of each layer to be described as $R_i = 2R_{\text{f},0}(1 + b_i K)$, where R_i is the resistance of the ith layer. Using the equation of parallel resistances the expected strained fiber resistance can be modelled as:

$$R_{\text{f}} = \frac{R_1 R_2}{R_1 + R_2} = \frac{4R_{\text{f},0}^2(1 + b_1 K) \cdot (1 + b_2 K)}{2R_{\text{f},0}(1 + b_1 K) + 2R_{\text{f},0}(1 + b_2 K))} \tag{A.21}$$

Finally the change in resistance can by calculated as follows:

$$\frac{\Delta R}{R_{f,0}} = \frac{R_{\mathrm{f}} - R_{\mathrm{f},0}}{R_{\mathrm{f},0}} = \frac{2b_1 b_2 K^2 + b_1 K + b_2 K}{2 + b_1 K + b_2 K} \tag{A.22}$$

These equations assume a linear resistance response to strain and are used to determine the gauge factor of the printed samples.

During previous research a bilinear resistace response to strain was measured [5, 6]. For small strain values the resistance increases linearly. This resistance change reversible. For larger deviations carbon fibers fracture resulting in an irreversible linear increase in resistance.

B Design

B.1 Introduction

This chapter will explain important considerations during the design process. The placement of the fibers using the slicer will be discussed as well as the method to make the electrodes. Additionally the phenomenon known as warping will be explained along with a possible solution. Finally the design of all the samples which have been tested will be explained.

B.2 Software limitations

The designed parts are printed on the Anisoprint A4 composer [7, 8]. To generate the G-Code for this printer the slicer (Aura 1.24.2 [9]) is used, which is a slicer made for the printing of continuous fibers. In the slicer the placement of the fibers can be determined using three different settings as seen in Figure B.1:

- Outer reinforced perimeter count.
- Inner reinforced perimeter count.
- Reinforced infill type.

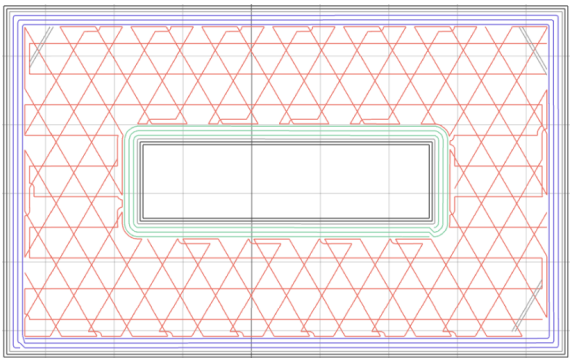

Figure B.1: Fiber placement options in the Aura slicer (Plastic (Grey), Outer fiber (Blue), Inner fiber (Green), Fiber infill (Red))

These settings can be adjusted for every model as well as for different height ranges. The outer reinforced perimeter setting places loops of carbon fiber around the outside of the part. This setting is most useful for simple fiber paths and provides the most strength per fiber since it is placed furthest away from the neutral plane. However, when the fiber should not follow the outer walls, e.g. to achieve a "zigzag" pattern of fiber inner reinforced perimeter can be used. By creating a thin inner void (≈ 0.1 mm) in the model of the desired fiber path, the slicer can place fibers around the inner void. It is important to keep in mind that the placed fibers form a loop around the void. All reinforced perimeters need to be placed in loops, which is a limitation in the slicer.

An other slicing limitation is the minimum fiber length of 45 mm. The carbon fiber needs to be cut before the end of the extrusion move, because it can not be separated using a simple retraction as conventional thermoplastics. This means that the length of the extruded fiber needs to be larger than the distance from the cutting blade to the tip of the nozzle, which is 45 mm. Otherwise the fiber would be cut before it exits the nozzle, which results in a clogged nozzle.

Finally, the slicer does not allow the fibers to be placed on the outside of the part. This means that every fiber has at least two perimeters of PETG around it, as seen in Figure B.1. Additionally, all samples have two PETG layers (in total 0.34 mm) at the top and bottom of the part.

B.3 Practical considerations

A common problem with 3D-printing is warping [10]. Warping describes the deformation of a printed part as is 'warps' from the print bed, resulting in a deformed final part. Usually this issue is caused by inhomogeneous cooling of the part while printing. When the extruded plastic cools down it contracts. The thermal contraction leads to internal stresses causing the part to warp. A solution to this problem is to use an adhesive, such as Magigoo [11], to help the plastic to stick to the bed. However, this method does not prevent internal stresses to occur, since the temperature of the part is not influenced. An other solution is to use a heated bed and an enclosure, which helps to stabilize the temperature. Only after the print is finished the entire part cools down at approximately the same speed. In this case the parts shrinks homogeneously with minimal distortion [10]. However, when printing with carbon-fiber this problem persists. Since the part consists of multiple materials (PETG and carbon-fiber), and both materials have different coefficients of thermal expansion(CTE), as seen in Table B.1, the final part does not shrink homogeneously, which results in warped parts as seen in Figure B.2.

One method to prevent warping is to position the fibers symmetrically inside the part. This way once the part cools down the internal stresses cancel each other.

Material	CTE [1/°C]
PETG	$68 \cdot 10^{-6}$
Carbon-fiber	$\approx 2 \cdot 10^{-6}$

Table B.1: CTE for the printed materials [12] [13]

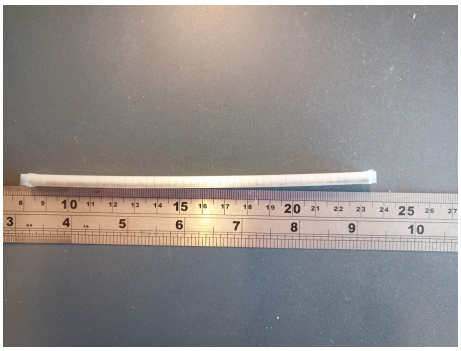

Figure B.2: Warping on single side sample

Another reason to place the fibers symmetrically within the part is to keep the neutral plane in the center. This simplifies the mechanical model and makes it possible to compare samples with different amount of reinforced perimeters. Asymmetric fiber placement could be used to optimize the sensitivity and stiffness of the part. By placing many fibers near the bottom of the part and a few near the top, the part will be stiffer and the neutral plane will be further away from the top fibers, which experience more strain, and thus a higher change in resistance.

B.4 Fabrication

The samples are printed on the Anisoprint Composer A4, which is an FFF 3D-printer with a secondary extruder for composite fiber co-extrusion (CFC) [7]. During this process, plastic is molten and extruded together with the carbon-fiber, which embeds the fiber inside the plas-

tic part as seen in Figure B.3. Varying the extrusion rate of the fiber filament and the plastic filament adjusts the fiber volume ration [14]. Different materials can be used around the fiber.

To prevent warping a thin layer of Magigoo [11] glue is placed on the glass print bed before printing.

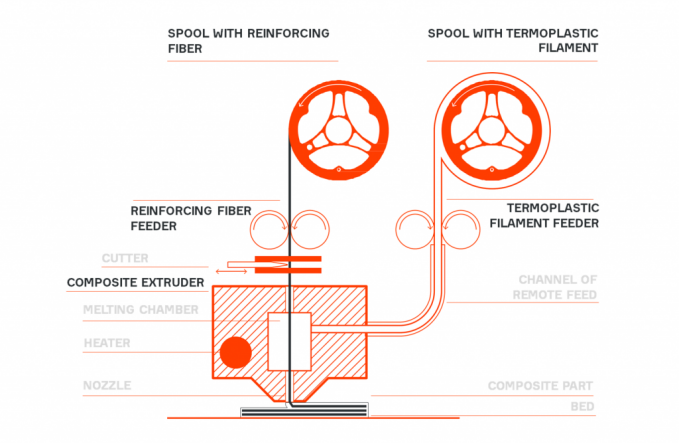

Figure B.3: Anisoprint Composite Fiber Co-extrusion technology [7]

B.4.1 Software

The geometry of the samples are designed in FreeCad v.0.19 [15]. As previously mentioned the slicer used to determine the fiber placement and generate the G-Code, is the Aura slicer [8, 9]. The default printing profiles for PETG and carbon-fiber filament are selected which contain the following settings:

Table B.2: Printing parameters

Printing parameter	Value
Bed temperature	60 °C
Nozzle temperature	240 °C
Extrusion width	0.65 mm
Extrusion multiplier	1
Infill Density	20% | 45%
Infill type	Triangles
PETG layer height	0.17 mm
CCF layer height	0.34 mm
PETG printing speed	50 mm s^{-1}
First layer speed	30 mm s^{-1}
CCF printing speed	5 mm s^{-1}

B.4.2 Sample geometry

For the experiments different samples have been used.

The first samples are used to determine the resistance of the printed fiber and a suitable method to make the electrodes. These are simple 10 mm × 30 mm × 45 mm cuboids with various amount of carbon-fiber specified using a height-range modifier, which can be seen in Figure B.4. The samples can be seen in Figure B.5, which shows each samples with two electrodes

made using silver-paint and two electrodes made using a stainless steel M2 bolt as explained in Section B.4.3.

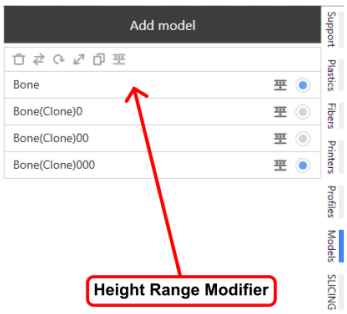

Figure B.4: Button for the height range modifier located under the Models tab.

The second set of samples as seen in Figure B.6 are used for a three point bending test as described in Section C.3. These samples are similar cuboids with an increased length of 150 mm. The fibers are all placed in the bottom 2 mm. Six different beams have been printed where each sample only differs in the reinforced perimeter count, which ranges from 0 to 5.

Finally, to keep the neutral plane in the center of the part and to simultaneously measure the fibers in compression (located in the top layers) and fibers in tension (located in the bottom layers) samples have been printed with fibers located symmetrically within the part. To be able to connect electrodes to the top and an bottom fibers individually the ends have been split into different directions, resulting in a Y-shape as depicted in Figure B.7. Additionally the center section of the sample has been lengthened to be 220 mm.

The number of fibers refers to the amount of fibers which make up the strain gauge. Since each perimeter forms a loop of which two sections are part of the strain gauge, two fibers are added per perimeter. It can be expressed as the following equation:

$$N_{\text{fibers}} = N_{\text{fiber layers}} \cdot N_{\text{fiber perimeters}} \cdot 2 \tag{B.1}$$

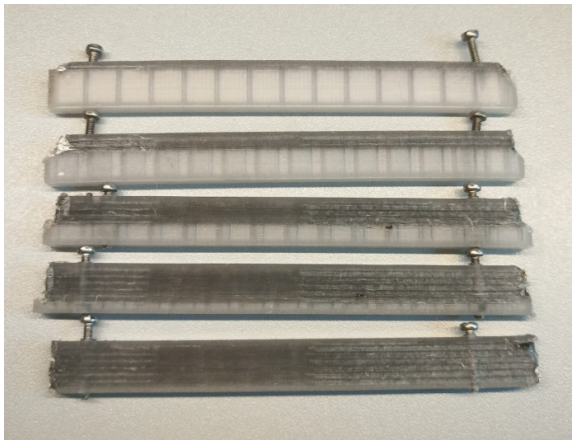

Figure B.5: Samples used for resistance measurements (Viewed from the side)

B.4.3 Electrode preparation

Once the parts have been printed the electrodes need to be prepared to be able to measure the resistance.

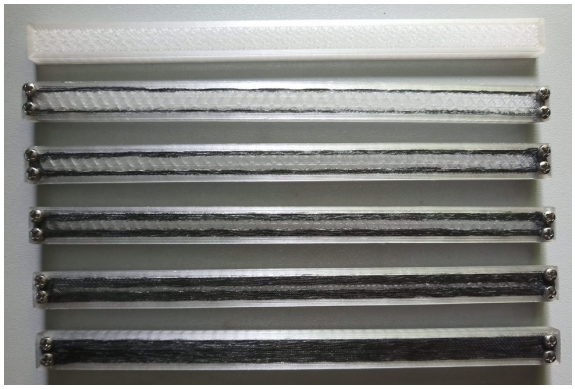

Figure B.6: Top view of samples with fibers only on one side ranging from zero up to five reinforced perimeters, used during resistance measurements and three-point-bending tests.

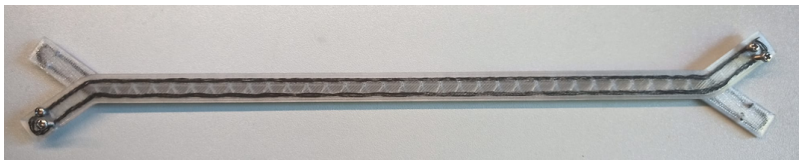

Figure B.7: Top view of sample with symmetric fiber placement with two layers of three reinforced perimeters, used for three-point-bending tests.

Making an electrical connection to the fibers has been a common problem in research, due to the high contact resistance [16]. This makes 2-point resistance measurement unpractical. Therefore, 4-point resistance measurements are required. Different techniques have been explored which include:

- Silver paint on exposed fiber
- Mechanical connection with a stainless steel screw
- Nickel electroplating
- Silver electroplating
- Silver epoxy
- Clamps on exposed fiber

During this study only the first two methods have been examined.

The first method requires the fibers to be exposed. Since PETG does not dissolve in the most commonly used solvents, e.g. acetone, ethanol and H_2SO_4 [17, 18], a soldering iron is used to melt away the plastic around the CCF. Furthermore, even if a usable solvent is found, it might not dissolve the plastic around the CCF composite filament, since its mixture is not known. Once the fibers are exposed, silver paint is applied. After the solvent of the silver-paint evaporates the sample can be used for measurements. Optionally, a wire can be added to the electrode by soldering it to a piece of copper tape and placing it slightly over the silver paint. Using more silver paint an electrical connection between the copper and the silver paint is made.

When using the second method a 1.5 mm hole is drilled barely touching the fibers, such that the fibers are exposed, but not cut apart as seen in Figure B.8. An M2 stainless steel bolt is screwed into the hole. Since the hole is undersized, the thread of the screw presses into the fibers making an electrical connection. This method is both faster and easier to implement compared to the first method of making the electrode.

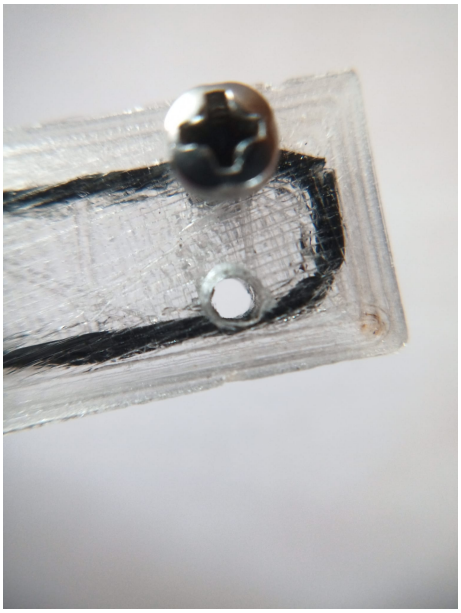

Figure B.8: 1.5 mm hole for the electrode touching the carbon-fiber

For all printed samples, with the exception of the samples used for the resistance measurements, the second method has been used, because of a lower contact resistance as described in Section D.2.2, and a faster and easier fabrication process.

C Experiments

C.1 Introduction

In this chapter the experiments mentioned in the paper will be explained in more detail. Furthermore, additional experiments, which are not discussed in the paper, will be explained.

C.2 Resistance Measurement

To determine the piezoresistive properties of 3D-printed continuous carbon-fiber the resistance needs to be measured. The Keithley 2000 multi-meter has been used to measure the resistance of the carbon-fiber using 2-point and 4-point resistance measurements.

C.2.1 4-point Measurement

Since the contact resistance from the electrodes to the CCF is significant, 4-point resistance measurements are required. As the name implies this measurement uses four electrodes, two current carrying electrodes and two electrodes to measure the voltage. Since the voltage is not measured across the current electrodes, the voltage drop caused by contact resistance and the resistance in the current carrying wires is not included in the measurement. This makes it possible to precisely measure small resistances ($R < 100\Omega$) [19].

As mentioned in the paper, parallel and diagonal 4-point measurements are used for the samples with four electrodes placed on a fiber loop. While these are not conventional 4-point resistance measurements, where all electrodes are placed inline with each other, the contact resistance remains excluded from the measurement.

C.2.2 Contact Resistances

To determine the contact resistance, the resistance of the fibers have been measured using the conventional 4-point resistance measurements and 2-point resistance measurements.

By calculating the difference between both measurements the contact resistance is determined. It should be noted that the resulting contact resistance is the sum of the resistance within the current carrying wires, the contact resistance from the wires to the electrodes and the main contact resistance from the electrodes to the carbon-fiber.

C.2.3 Composite-carbon-fiber filament

To determine the electrical properties of 3D-printed carbon-fiber, first the resistance of the single strand of composite-carbon-fiber filament is measured. Since the filament is a composite of plastic and carbon fiber, it is not possible to directly make electrical contact with the fibers. First the fibers need to be exposed by burning the plastic with a lighter leaving only the raw fibers as seen in Figure C.1.

Using a conventional 4-point measurement the resistance of a single fiber-strand is determined. To make sure that the voltage drop is proportional to the current it has been measured at various currents ranging from 5 mA to 100 mA.

C.2.4 Resistance of fibers inside a loop

The neutral resistance of the fibers making up the strain gauge $R_{f,0}$ can be calculated using the Equation A.17. Therefore, the resistance of the single-side samples and the resistance of the symmetrical samples have been measured using both diagonal and parallel 4-point resistance measurements.

Figure C.1: Exposed fibers inside filament

C.3 Three point bending test

The three-point-bending test is a standardized test, often used to measure the modulus of elasticity of a homogeneous beam in bending. Since the 3D-printed beams are not homogeneous, the stiffness is measured instead, which is compared to the expected stiffness resulting from the mechanical model.

The test is performed by placing a sample on two round supports, with a radius of 5 mm. The distance between the support depends on the size of the samples. For the single side samples, which have a length of 150 mm, the supports are placed 120 mm apart, and similarly for the symmetric samples with a center length of 220 mm the supports are placed 200 mm apart.

A load is applied on the sample midway between the supports to bend the sample. [20, 21].

The linear actuator used to apply the force is the SMAC (LCA25-050-15F, Figure C.2), which can apply a force to the sample up to 12 N. During a single test the force linearly increases from 0 N to 12 N and then decreases at the same rate back down to 0 N. This cycle has a period of 10 s and is repeated ten times to account for noise, hysteresis and creep.

The deflection of the beam is measured by the SMAC, using its position sensor. And the resistance of the fibers within the part is measured using a diagonal 4-point resistance measurement on the Keithley 2000 to circumvent the contact resistance problem as mentioned in Chapter A.

During the tests the time, position, force, and resistance is saved at a rate of ≈10 Hz. This frequency is limited by the measuring rate of the multi-meter. To control the SMAC and read data from the multi-meter, the devices are connected to a computer running Matlab. A schematic of the entire setup can be seen in Figure C.3.

For the symmetrical samples additional measurements are performed, where the resistances of the top and bottom strain gauges are measured simultaneously. An HP 34401A multi-meter measures the resistance of the strain gauge under compression, while the Keithley 2000 measured the resistance of the strain gauge under tension. Subtracting the compressive resistance from the tensile resistance simulates a differential measurement.

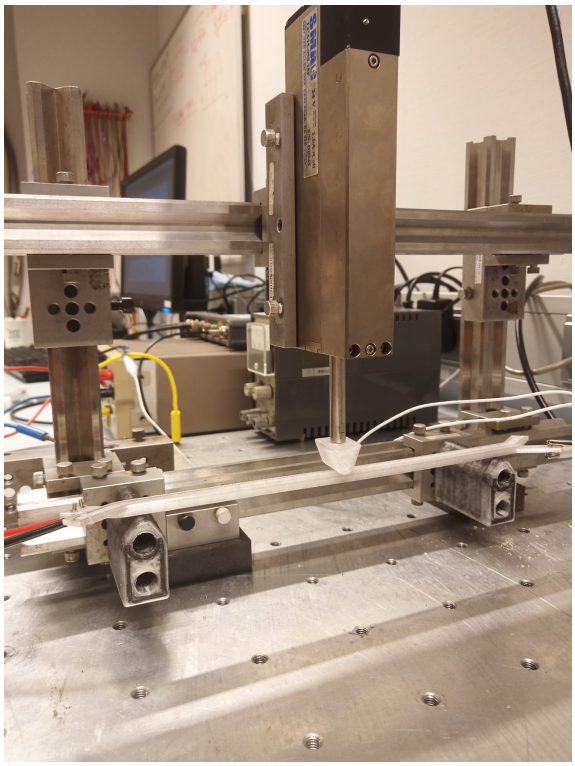

Figure C.2: Experimental setup for 3-Point Bending test showing the SMAC actuator and a symmetrical sample placed on the supports.

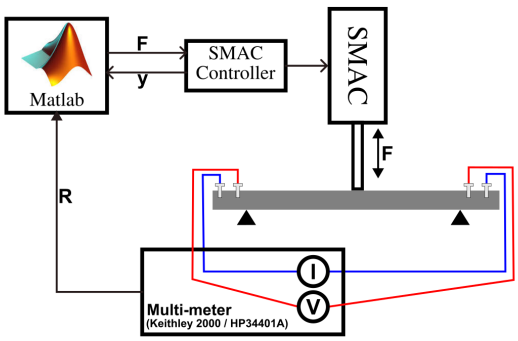

Figure C.3: Schematic Diagram of 3-Point Bending test setup

D Results

D.1 Introduction

In this chapter additional measurement results will be shown and explained.

D.2 Resistance Measurements

D.2.1 Composite-carbon-fiber filament

The resistance of a single of CCF composite filament has been measured as explained in Section C.2.3:

$$R_{\text{filament}} = 116\Omega \tag{D.1}$$

The distance between the voltage electrodes on the fiber was 360 mm, which means that every centimeter adds approximately 3.22 Ω of resistance.

Additionally the voltage measurement at different current levels as seen in Figure D.1 confirms the expected linear correlation, with a coefficient of determination of $R^2 = 0.99996$.

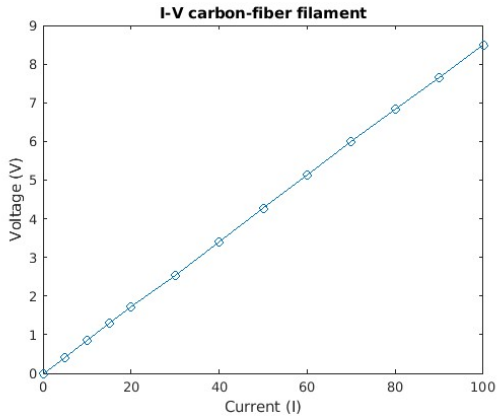

Figure D.1: Correlation between Current and Voltage for composite-carbon-fiber filament

D.2.2 Contact resistance

The contact resistance measured for the two different methods described in Chapter B can be seen in Figure D.2. It clearly shows that the contact resistance is lower when using the second method, screwing a stainless steel bolt into the fiber. Additionally there seems to be a correlation between the contact resistance and reinforced perimeter count. This makes sense since increasing the amount of reinforced perimeters increases the contact area, which results in a lower contact resistance.

D.2.3 3D printed carbon fiber

The resistance of all samples have been measured and the results can be seen in Figure D.3. It shows the measured fiber resistances of all samples, as well as the expected resistance.

The figure shows that most measured resistances roughly matches the expected value. This allows the resistance of the final part to be estimated with the parallel resistor equation. Most values are slightly larger than the expectation, which can have many different causes, which will be elaborated in the discussion.

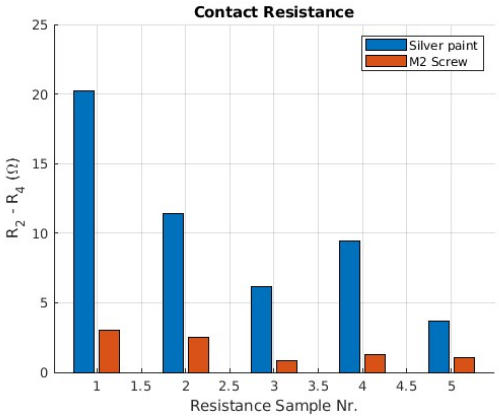

Figure D.2: Contact Resistance measurements

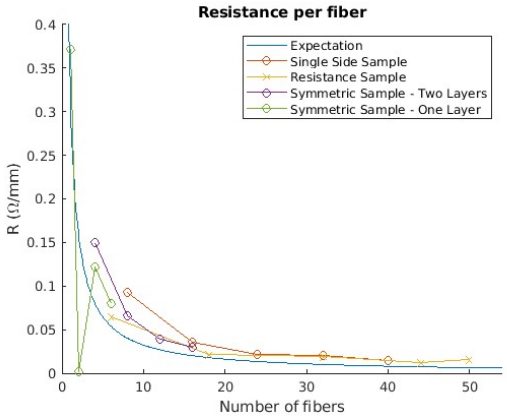

Figure D.3: Neutral resistance of strain fibers compensated for orthogonal resistance R_x

D.2.4 Orthogonal resistance

The relative orthogonal resistances of the samples for the three-point-bending test has been determined using Equation A.17, as seen in Figure D.4.

The relative orthogonal resistance R_x/R_f is lower for the symmetrical samples compared to the single side samples. This difference can be explained by the different lengths. The symmetrical samples have a length of 26 cm compared to the 15 cm of the single side samples. Since R_f is proportional to the length the relative orthogonal resistance is lower for the symmetrical samples. Additionally R_x varies significantly for each sample.

D.3 Three point bending results

A three layered mechanical model is fitted to the stiffness of the sample containing 120 fibers to determine the value, which is applied to the mechanical models for the other samples to predict the expected stiffness. The fitted Young's modulus of the CCF is:

$$E_{CCF} = 57.45\text{GPa} \tag{D.2}$$

Which is 43 % of the value found in the data-sheet of the CCF composite filament [7].

D.3.1 Single Side Samples

The resistance of the samples containing CCF on only one side are tested during three-point-bending tests. Figure D.6 shows in the left graph, that the stiffness increase as a function of the number of fibers in the sample is non-linear. This is a result of a shifting neutral plane.

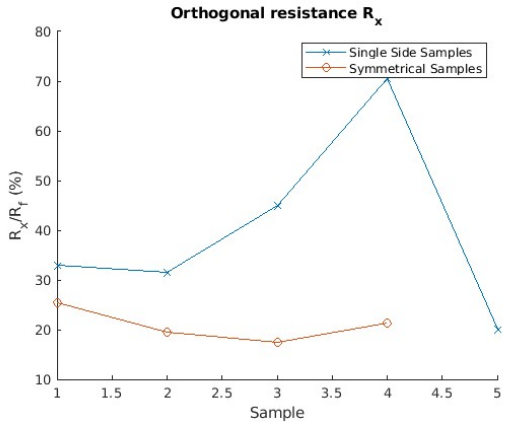

Figure D.4: Relative orthogonal resistance R_x for single side samples and two layered symmetrical samples

When adding more fibers to one side, the neutral plane shifts towards the fibers as seen, which is confirmed by the model which matches the stiffness measurement.

On the right graph the relative resistance change, compensated for the orthogonal resistance R_x, is shown. Only the samples with one and two perimeters show a significant change in resistance. When increasing the amount of reinforcement fibers, the neutral plane shifts to within the CCF as seen in Figure D.5. Because the resistance change is proportional to the strain. Once the neutral plane is within the CCF almost no strain is expected inside the fibers. Therefore almost no change in resistance is expected.

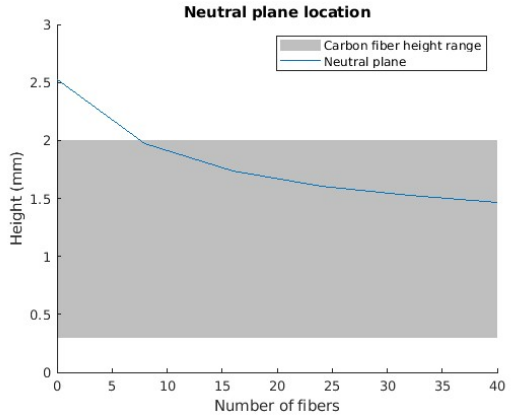

Figure D.5: Modelled height of the neutral plane for one sided samples

D.3.2 Symmetric Samples

The time plots of the symmetric samples can be seen in Figure D.7, which shows the triangular actuation force, the center deflections and the resistances of the top and bottom strain gauges. Due to an increasing stiffness the peaks of the center displacement are decreased. The bottom strain gauge, which is under tension, shows an increase in resistance, whereas the resistance of the top strain gauge, which is under compression, decreases.

The stiffness results of the samples are shown in Figure D.8. Since the CCF is placed symmetrically the neutral plane remains in the center which is confirmed by the linear stiffness increase. The slope of the samples containing a single fiber layer is larger since the average distance from the fibers to the neutral plane is larger.

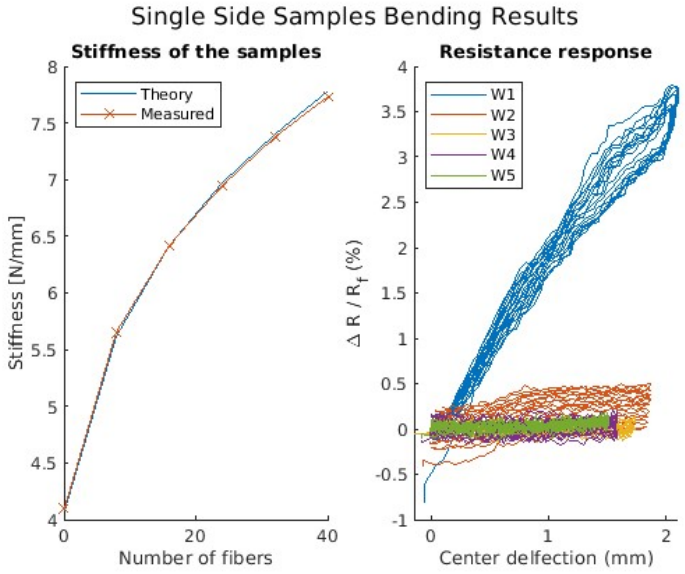

Figure D.6: Stiffness of the samples and the modelled expectation (Left); Resistance response (Right)

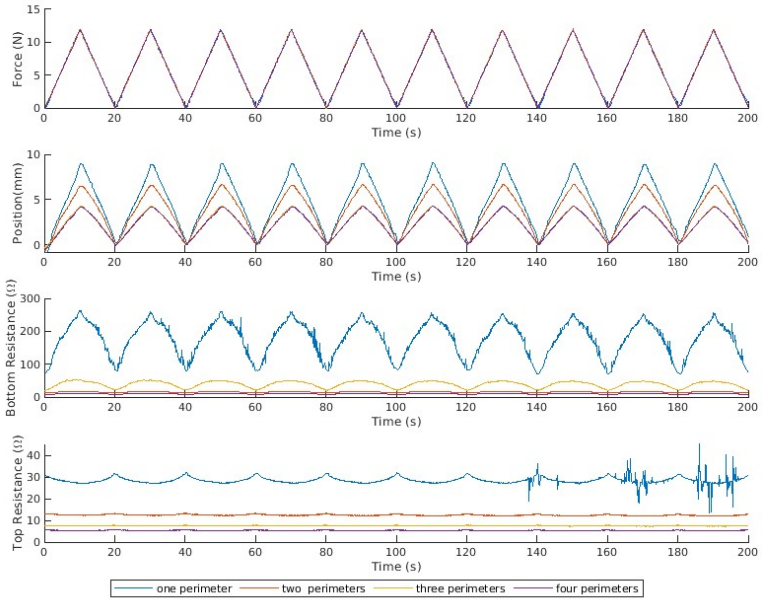

Figure D.7: Time plots of a two-sided measurement for samples with two fiber layers; (top) actuation force,(top-center) center defection, (bottom-center) resistance of strain gauge in tension; (bottom) resistance of strain gauge in compression

During the first three-point-bending measurements only small resistance changes have been measured as seen in Figure D.9. These results noise and drift, but do not indicate a strain dependent resistance.

Later measurement with the same samples show significant strain dependent resistance as seen in Figure D.10. The resistance change is significantly larger during tensile measurements compared to compressive measurements. These sample show high noise levels of $\approx \pm 2\,\%$.

Since there is no axial strain during a three-point-bending test, the expectation for the sum of the resistances is a flat line, if the strain response during compression is the same as under

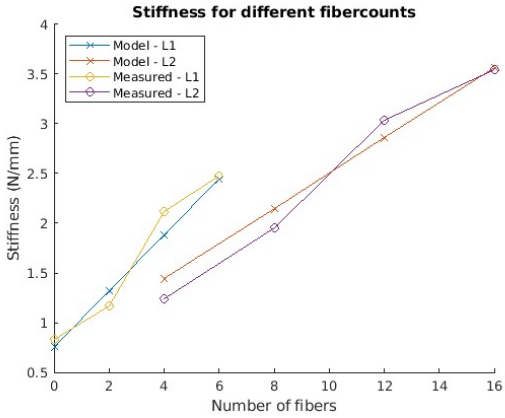

Figure D.8: Stiffness measurements and expectation of symmetric samples

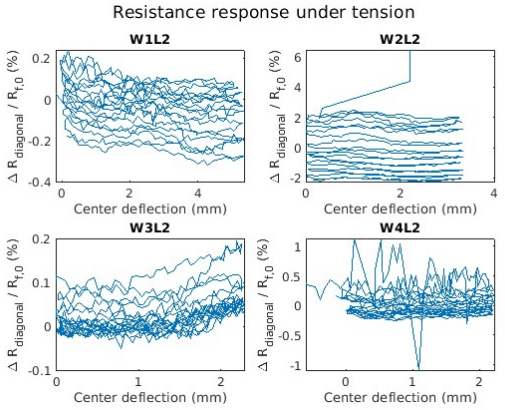

Figure D.9: Initial strain-dependent resistance measurements of strain-gauge printed close to the print bed compensated for orthogonal resistance R_x

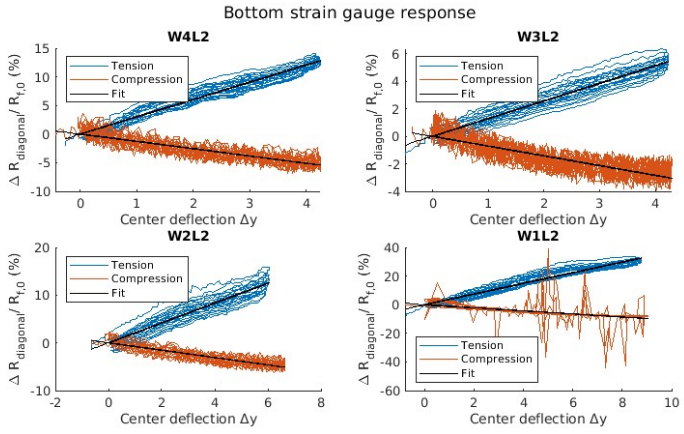

Figure D.10: Tensile and compressive resistance measurement of strain-gauge printed close to the print bed during three-point-bending test compensated for orthogonal resistance R_x

tension. This expectation is not seen in Figure D.11, which means that the strain response is not the same on the compression and tension side.

The gauge factors as seen in Figure D.12 show a significantly higher sensitivity under tension compared to compression.

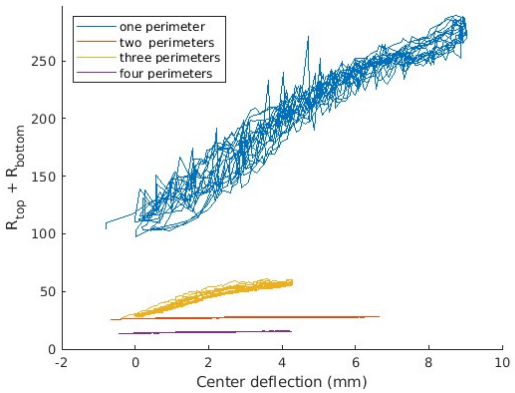

Figure D.11: Sum of the top and bottom strain gauge resistance for different samples

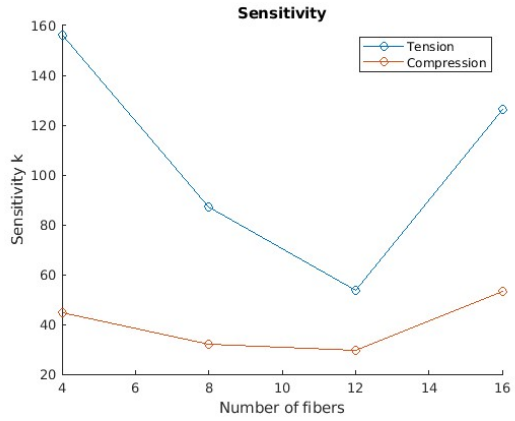

Figure D.12: Gauge factors determined for measurements in Figure D.10

E Discussion

In this chapter the main findings will be discussed and their possible causes will be explained.

E.1 Quality of 3D-printed fibers

The Anisoprint Composer A4 printed all experiment samples. The plastic printing performance is good, and results in accurate parts with consistent extrusions.

However, while printing the CCF composite filament some issues arise. For example the placed fibers are not straight as seen in Figures B.6 and B.7, even though the G-Code paths are straight lines. This could be caused by the printing profile selected for the CCF, which uses an extrusion width of 0.65 mm. Because the diameter of the carbon fiber is 0.35 mm, the fiber needs to be 'over-extruded' resulting in non straight fibers. By tuning the printing profile this problem could be resolved. Another problem is the beginning and the ending of a reinforced perimeter. It is possible that the ends of the placed fiber do not touch, which results in an open circuit, as seen in Figure E.1. Future slicer updates could include a setting to overlap the beginning and the end of a fiber-placement.

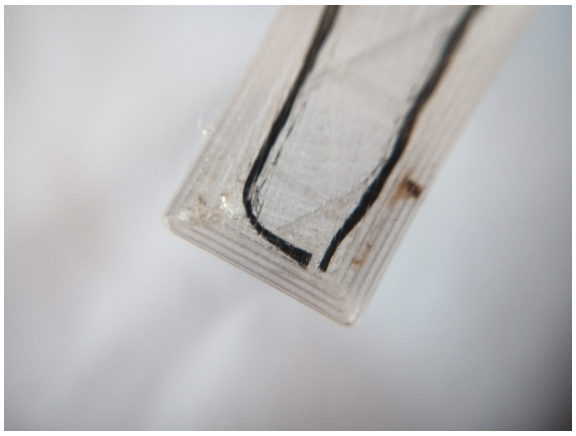

Figure E.1: Sample with one reinforced perimeter where the ends of the fiber loop are not properly connected

E.2 Higher resistance measurement

As shown in Chapter D, the calculated values for the fiber resistance are following a similar curve as the expectation, but are slightly higher. The results show that the fiber resistance can be estimated using the resistance of the unprinted fiber. Multiple factors can cause the calculated value to be higher. It is possible that the printing process slightly increases the resistance of the printed fibers. During the fabrication some fibers could have been damages resulting in a higher resistance. The two dimensional resistance in between the fibers can cause an uneven current distribution. This effect is not taken into account by the model, just like the consequences of asymmetrical orthogonal resistances, which could cause measuring deviation.

E.3 Orthogonal resistance

The orthogonal resistance R_x is an unwanted consequence of 4-point resistance measurement on reinforced perimeters, which form a loop. Because of this parallel and diagonal 4-point resistance measurements are required to determine the strain gauge resistance.

However, the fiber loop can be an advantage, since it could be used as a 3D-printed Wheatstone bridge. A diagonal 4-point resistance measurement is essentially the same as Wheatstone

bridge with a current source instead of a voltage source, as shown in Figure E.2. Using a voltage source instead of a current source, the bridge voltage would be:

$$V_{\text{bridge}} = V_{\text{in}} \frac{R_{\text{f}} - R_{\text{x}}/2}{R_{\text{f}} + R_{\text{x}}/2} \tag{E.1}$$

This means that by tuning the ratio between R_{x} and R_{f}, e.g. by changing the lengths of each section through strategically placed electrodes, the sensitivity can be optimized. Future research could investigate the feasibility of such optimization techniques.

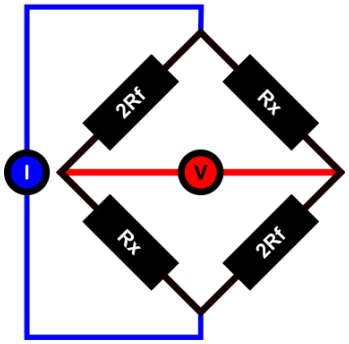

Figure E.2: Diagonal 4-point resistance measurement as a Wheatstone bridge

The model used for the resistance uses two important assumptions as mentioned in Chapter A. The assumption that the orthogonal resistance remains constant during the three-point-bending test has not been tested during this research. The second assumption is required to be able to calculate the resistance of the strained fibers. Figure E.1 shows that this assumption is not always correct and Figure D.4 shows that the orthogonal resistances are not consistent.

Overall the orthogonal resistance bears the same problems as contact resistances, such as a resistance offset, where the contact resistance could be modelled as a constant positive offset and the orthogonal resistance is a measured as a constant negative offset during a diagonal 4-point resistance measurement. Additionally, it is not clear whether either resistance changes during the three-point-bending test. Therefore, for the sole purpose of measuring the strained fiber resistance a 2-point measurement would be better, since it is easier to model, fabricate and does not include more uncertainties than the orthogonal resistance.

E.4 Low effective strength of continuous carbon fiber

The stiffness measurement indicates that the continuous carbon fibers only provide 43 % of the expected strength. This is consistently confirmed by the mechanical model for the single side and symmetrical samples, where the model matches the measurement. Even though the Young's modulus has been chosen as the fit parameter, the result includes the error in the estimated fiber volume fraction and the strength reduction due to inconsistent fiber placement while 3D-printing. Currently the fiber volume fraction is estimated by the cross-sectional area and the amount of printed fibers. However it plausible that the printed cross sectional area does not match the filaments cross sectional area, resulting in a lower fiber volume fraction. For a better estimation of the fiber volume fraction many slicing settings should be taken into account, such as extrusion width and plastic co-extrusion ratio.

E.5 Increasing sensitivity for second measurement

Figures D.9 and D.10 show the results of the same experiment at different times. The first results show the response after the electrodes have been fabricated, before the sample experienced any bending. Since these measurements did not match the expectation the sample was bent manually. During the manual bending significant resistance changes have been observed.

Afterwards the results in Figure D.10 have been measured, which show significantly higher resistance changes and noise.

The only significant difference between the two measurements is the manual bending. During the manual bending small cracking noises can be an indication of fiber fracture. Since the manual bending forces exceed the actuation force during the measurement, more fibers are fractured after bending. It is possible that the resistance response seen in Figure D.10 could be caused by the fractured fibers. This seems to indicate a correlation between the sensitivity of the strain gauge and the fiber fractures. However, previous research describes fiber fractures as irreversible resistance changes, which does not fit with the measured reversible resistance changes.

E.6 Large resistance changes

During the three point bending tests large resistance changes have been measured which result in a gauge factor of $k > 150$. Since the electrodes extend past the three-point-bending supports, a fraction of R_f is measured, but does not experience any strain. Which means the actual sensitivity of the strained fiber is higher than the measurements.

Overall the measured sensitivity is much larger than usual CCF gauge factors which range from $-5 < k < 5$ [22]. At the Brightlands material center they have measured similar resistance changes over 100 % [23]. The exact reason such high resistance changes were measured us not clear, however, multiple factors could play role.

One of these factors is the CCF composite filament made by Anisoprint, which has been used for this research. This filament is specifically made for 3D-Printing and is impregnated with a thermoplastic polymer. Unfortunately, the exact composition of the plastic and the manufacturer of CCF are unknown. To the authors best knowledge this composite filament has only been used to measure strain by the Brightlands material center. Therefore, it is plausible that the cause of these resistance measurements is the CCF composite filament. Additionally, possible fiber fractions causing a change in sensitivity could also be responsible for large resistance changes.

E.7 High noise levels

The results in Figures D.9 and D.10 both show significant levels of noise, which make these strain gauges unpractical for precise sensing of small deflections.

Electromagnetic interference could be a possible source of this. Because the resistance or the fibers are small, it could function as an antenna and receive the 50 Hz AC-Signal from nearby outlets. Since the sampling rate is ≈10 Hz the signal would be measured as noise. By measuring the frequency at a higher sampling rate above 100 Hz, the significance of this effect can be determined.

Another explanation of the noise are the individual carbon fibers. Since the CCF composite filament consists of many individual fibers, inter-fiber connections could arise or break resulting in a stochastic signal. Fiber-fraction would increase the amount of fibers and therefore the amount of inter-fiber connections, which would explain why there is more noise in Figure D.10 than in Figure D.9.

E.8 Mechanical model

Properties of the 3D-printed beam can b determined by the mechanic model work, e.g. the expected stiffness matches the measured stiffness of each sample. There are small deviation for the symmetrical samples. Different amounts of fiber fractions could explain this, but more research on this is required.

Due to the large difference between the Young's moduli of plastic and CCF, the height ranges of each material are important. Excluding the influence of two plastic top and bottom layers causes a significant deviation. The model could be improved by finding a better method of estimating the fiber volume fraction and to include the co-extruded plastic around the fiber.

E.9 Piezoresistive Model

The piezoresistive model, as explained in Chapter A, provides a linear model for the strain response to determine the gauge factors. The piezoresistive model does not depend on the number of fibers and the measurements seen in Figure D.12 do not indicate a clear correlation. A negative correlation between the number of fibers and the sensitivity is expected, since more fibers increase the changes of inter-fiber connections during bending, which decrease the overall resistance. However, the correlation is expected to be insignificant compared to factors such as the fiber volume fraction, fiber pretension and fractured fibers, which could all be important topics for future research.

Due to the different strain in different layers the extended model was determined, however, the noise in the measurements exceeds the influence of the different layers. Since the sensitivity of the samples is inconsistent and does not match previous research [5], it is difficult to determine the performance of the piezoresistive model.

F Conclusion

This report has described the theoretical framework for characterizing 3D printed CCF reinforced beams, by making a mechanical model and an electrical model. Important considerations on how to use the software to prepare the G-Code for the samples as well as considerations to ensure a successful print were explained. Experimental methods to test the samples along with the measured results were discussed and finally different causes of important findings have been explored.

A good method to fabricate strain gauges for these measurements has been found during the study and is listed as a set of guidelines:

- Place the fibers symmetrically inside the part to keep the neutral plane in the center and prevent warping
- Use the reinforced perimeter setting in the slicer for the most control on the position of the fibers
- Use at least two reinforced perimeters and fiber layers to prevent issues with unreliable electrodes
- Place the electrodes on the same fiber, to minimize 2D resistance.
- Try to use conventional, inline, 4-point resistance measurements to directly measure the fiber resistance

Having tested multiple different carbon-fiber reinforced beams using three-point-bending tests, the stiffness of each beam was found to match the mechanical model. The resistance measurements show a lot of potential for practical sensing application, due to a high sensitivity. However, the piezoresistive model can not predict the sensitivity, instead, it can only be used to determine the sensitivity based on the measurements. The noise measured during the three-point-bending tests make these strain gauges not suitable to measure small deflections without further research on the cause and possible solutions. No significant correlation between the sensitivity and the number of fibers has been found.

There are many possibilities for future research, such as the characterization of the CCF filament, optimizing the slicing settings for electrical connections or determining the source of the high noise levels. However, the influence of fiber-fractures on the stiffness, noise, resistance and sensitivity seems most interesting, since it could explain almost all unexpected findings during this study.

Bibliography

[1] R. C. Hibbeler, S. C. Fan, and P. Schiavone, *Engineering mechanics : statics*. Singapore: Prentice Hall, 12th ed. in si units / ed., 2010.

[2] R. Hibbeler, *Deflection and Elastic Beam Theory*, vol. 8. Prentice Hall.

[3] S. K. F. Ansel C. Ugural, *Advanced Mechanics of Materials and Applied Elasticity*. Peasron, 6 ed., 8 2019.

[4] K. Gramoll, "Mechanics ebook: Composite beams." www.ecourses.ou.edu/cgi-bin/ebook.cgi?topic=me&chap_sec=06.1&page=theory. 7 Jun 2022.

[5] C. Luan, X. Yao, H. Shen, and J. Fu, "Self-sensing of position-related loads in continuous carbon fibers-embedded 3d-printed polymer structures using electrical resistance measurement," *Sensors*, vol. 18, no. 4, 2018.

[6] C. Luan, X. Yao, C. Liu, L. Lan, and J. Fu, "Self-monitoring continuous carbon fiber reinforced thermoplastic based on dual-material three-dimensional printing integration process," *Carbon*, vol. 140, pp. 100–111, 2018.

[7] Anisoprint, "Anisoprint Composer." https://anisoprint.com/solutions/desktop/. (accessed: 16.03.2022).

[8] Anisoprint, "Anisoprint composer - manual." https://support.anisoprint.com/composer/manual/. 1 Jul 2022.

[9] Anisoprint, "Aura." anisoprint.com/aura/. 7 Jun 2022.

[10] K. Singh, "Experimental study to prevent the warping of 3d models in fused deposition modeling," *International Journal of Plastics Technology*, vol. 22, pp. 177–184, Jun 2018.

[11] Magigoo, "Magigoo." https://magigoo.com. 13 Jun 2022.

[12] SD3D, *PETG (Polyethylene terephthalate copolyester) Technical Data Sheet*, 2022.

[13] C. Dong, K. Li, Y. Jiang, D. Arola, and D. Zhang, "Evaluation of thermal expansion coefficient of carbon fiber reinforced composites using electronic speckle interferometry," *Opt. Express*, vol. 26, pp. 531–543, Jan 2018.

[14] F. Antonov, "Continuous fiber 3d printing: current market review by fedor antonov, ceo anisoprint." https://3dprintingindustry.com/news/continuous-fiber-3d-printing-current-market-review-by-fedor-antonov-ceo-anisoprint-164964/. November 18th 2019.

[15] FreeCad, "Freecad." https://www.freecad.org. 13 Jun 2022.

[16] P. Scholle, S. Rüther, and M. Sinapius, "Comparison of electrical contacting techniques to carbon fiber reinforced plastics for self-strain-sensing applications," *C*, vol. 7, no. 4, 2021.

[17] K. S. Erokhin, E. G. Gordeev, and V. P. Ananikov, "Revealing interactions of layered polymeric materials at solid-liquid interface for building solvent compatibility charts for 3d printing applications," *Scientific Reports*, vol. 9, p. 20177, Dec 2019.

[18] I. T. Heikkinen, C. Kauppinen, Z. Liu, S. M. Asikainen, S. Spoljaric, J. V. Seppälä, H. Savin, and J. M. Pearce, "Chemical compatibility of fused filament fabrication-based 3-d printed components with solutions commonly used in semiconductor wet processing," *Additive Manufacturing*, vol. 23, pp. 99–107, 2018.

[19] Wikipedia, "Four-terminal sensing." https://en.wikipedia.org/wiki/Four-terminal_sensing. 9 Jun 2022.

[20] "Iso-178 ;plastics — determination of flexural properties," 2019.

[21] Wikipedia, "Three-point flexural test." en.wikipedia.org/wiki/Three-point_flexural_test. 3 Oct 2021.

[22] P. Scholle and M. Sinapius, "A review on the usage of continuous carbon fibers for piezoresistive self strain sensing fiber reinforced plastics," *Journal of Composites Science*, vol. 5, no. 4, 2021.

[23] Brightlands Material Center, "Brightlands materials center develops self-sensing in 3d printed fiber reinforced thermoplastics." https://www.brightlandsmaterialscenter.com/self-sensing-in-3d-printed-thermoplastic-composites/. (accessed: 16.03.2022).